

1 **The Ca²⁺ sensor STIM1 regulates type I interferon response by retaining**
2 **the signaling adaptor STING at the endoplasmic reticulum**

3 **Sonal Srikanth^{1, 14, 15, *}, Jin Seok Woo^{1, 14}, Beibei Wu¹, Yasser M. El-Sherbiny^{2, 3, 4}, Jennifer**
4 **Leung¹, Koollawat Chupradit^{5, 6, 7}, Laura Rice⁸, Gil Ju Seo⁹, Guillaume Calmettes¹⁰, Chandran**
5 **Ramakrishna¹¹, Edouard Cantin¹¹, Dong Sung An^{5, 6, 7}, Ren Sun¹², Ting-Ting Wu¹², Jae U. Jung⁹,**
6 **Sinisa Savic^{2, 13}, and Yousang Gwack^{1, 15 *}**

7 ¹ Department of Physiology, David Geffen School of Medicine, UCLA, Los Angeles, California, USA

8 ² National Institute for Health Research—Leeds Biomedical Research Centre and Leeds Institute of Rheumatic
9 and Musculoskeletal Medicine (LIRMM), Wellcome Trust Brenner Building, St James's University Hospital,
10 Beckett Street, Leeds, UK

11 ³ Clinical Pathology Department, Faculty of Medicine, Mansoura University, Egypt.

12 ⁴ School of Science and Technology, Department of Biosciences, Nottingham Trent University, Nottingham, UK

13 ⁵ Division of Hematology-Oncology, David Geffen School of Medicine at UCLA, Los Angeles, California, USA

14 ⁶ School of Nursing, University of California at Los Angeles, Los Angeles, California, USA

15 ⁷ UCLA AIDS Institute, Los Angeles, California, USA

16 ⁸ Leeds Institute of Biomedical and Clinical Sciences, University of Leeds, Wellcome Trust Brenner Building, St
17 James's University Hospital, Beckett Street, Leeds, UK

18 ⁹ Department of Molecular Microbiology and Immunology, Keck School of Medicine, University of Southern
19 California, Los Angeles, California, USA

20 ¹⁰ Department of Medicine (Cardiology), David Geffen School of Medicine at UCLA, Los Angeles, California,
21 USA

22 ¹¹ Department of Molecular Immunology, City of Hope Beckman Research Institute, Duarte, California, USA

23 ¹² Department of Molecular and Medical Pharmacology, UCLA, Los Angeles, California, USA

24 ¹³ Department of Clinical Immunology and Allergy, St James's University Hospital, Leeds, UK

25 ¹⁴ Equal contribution

26 ¹⁵ Senior author

27 * Corresponding author

28
29 Address correspondence to: Dr. Sonal Srikanth or Dr. Yousang Gwack
30 email: ssrikanth@mednet.ucla.edu; ygwack@mednet.ucla.edu

32 **STING is an endoplasmic reticulum (ER) signaling adaptor that is essential for the type I**
33 **Interferon response to DNA pathogens. Aberrant activation of STING is linked to the pathology**
34 **of autoimmune and autoinflammatory diseases. The rate-limiting step for the activation of**
35 **STING is its translocation from the ER to the ER–Golgi intermediate compartment. Here we**
36 **found that deficiency in the Ca²⁺ sensor STIM1 caused spontaneous activation of STING and**
37 **enhanced expression of type I interferons under resting conditions in mice and a patient**
38 **suffering from combined immunodeficiency. Mechanistically, STIM1 associated with STING to**
39 **retain it in the ER membrane, and co-expression of full-length or a STING-interacting fragment**
40 **of STIM1 suppressed the function of dominant STING mutants that cause autoinflammatory**
41 **diseases. Furthermore, deficiency in STIM1 strongly enhanced the expression of type I**
42 **interferons after viral infection and prevented the lethality of infection with a DNA virus in vivo.**
43 **This work delineates a STIM1–STING circuit that maintains the resting state of the STING**
44 **pathway.**

45

46 The endoplasmic reticulum (ER) provides a structural platform for activation of the type I interferon
47 (IFN) response. Stimulator of interferon genes (STING), a key signaling adaptor protein for DNA-
48 sensing pathways localizes to the ER membrane in the resting state^{1, 2, 3}. After activation by cytosolic
49 DNAs, it translocates into the ER-Golgi intermediate compartment (ERGIC) to recruit TANK-binding
50 kinase 1 (TBK1) and interferon regulatory factor 3 (IRF3). IRF3, upon phosphorylation by TBK1,
51 homo-dimerizes and translocates into the nucleus to induce transcription of type I IFNs^{4, 5, 6, 7}. Beside
52 an essential role in protecting the host against DNA pathogens, STING is also involved in the
53 pathogenesis of autoinflammation caused by self-DNAs in murine models^{8, 9}. Accordingly, STING has
54 been implicated in the pathogenesis of Aicardi–Goutieres syndrome (AGS), systemic lupus
55 erythematosus (SLE) and other type I Interferonopathies¹⁰. Furthermore, mutations in STING have
56 been uncovered in patients with STING-associated vasculopathy with onset in infancy (SAVI) and
57 lupus-like symptoms^{11, 12, 13}. The STING variants found in SAVI patients are constitutively active and

58 localize to the ERGIC without the STING ligand, cyclic dinucleotides (CDNs), suggesting that they
59 may escape a mechanism that potentially maintains the ER localization of STING¹⁴. Since CDNs can
60 be generated by cytosolic self-DNAs derived from mitochondrial damage or genomic instability, and
61 the binding affinity of STING for CDNs is high (~5 nM for 2',3' cyclic guanosine monophosphate-
62 adenosine monophosphate [2',3'-cGAMP])¹⁵, active inhibitory mechanisms are necessary to tightly
63 control its activation. However, little is known about how the resting state of STING is maintained.

64 High Ca^{2+} concentration in the ER ($[\text{Ca}^{2+}]_{\text{ER}}$) is essential for its normal function. At the same
65 time, diverse receptors elevate cytoplasmic $[\text{Ca}^{2+}]$ by depleting ER Ca^{2+} stores through a mechanism
66 called store-operated Ca^{2+} entry (SOCE). Stromal interaction molecule 1 (STIM1), an EF-hand-
67 containing Ca^{2+} -binding protein localizes throughout the ER when $[\text{Ca}^{2+}]_{\text{ER}}$ is high, but after depletion
68 of the ER Ca^{2+} stores, it translocates into junctional areas between the ER and plasma membrane,
69 interacts with the pore subunit of store-operated Ca^{2+} (SOC) channels; Orai1, and induces Ca^{2+}
70 entry¹⁶. The essential role of STIM1 in effector function of adaptive immune cells including T and B
71 cells has been well established^{17, 18, 19}. Mutations in *STIM1* cause severe combined immune deficiency
72 (SCID) in humans²⁰. Paradoxically, these patients also suffer from lymphoproliferative and
73 autoimmune complications. Although for some forms of SCID, the mechanisms behind these
74 complications have been worked out; for example, poor development of both central and peripheral
75 tolerance²¹, the underlying causes of inflammatory complications in patients harboring mutations in
76 *STIM1* are not unknown.

77 The role of STIM1 in cells of the innate immune system is currently unclear. Here, we
78 examined the phenotypes of STIM1-deficient cells and observed that loss of STIM1 induces
79 spontaneous activation of the STING-TBK1-IRF3 pathway to activate type I IFN responses under
80 sterile conditions in both murine and human cells. Mechanistically, STIM1 directly interacted with
81 STING to retain it in an inactive state on the ER membrane. Accordingly, we also observed strong
82 resistance to viral infections in STIM1 KO cells and animals. These results suggest that STIM1 plays

83 an important role in regulation of the innate immune responses in addition to its well-established
84 function in regulation of SOCE in adaptive immunity.

85 **Results**

86 **STIM1 deficiency induces type I IFN response**

87 To gain insights into possible role of STIM1 in innate immune responses, we checked expression of
88 various inflammatory cytokines in *Stim1*^{-/-} murine embryonic fibroblasts (MEFs). Among these,
89 transcripts of *Ifnb1* and *Il6* as well as interferon-stimulated genes (ISGs) were significantly increased
90 in *Stim1*^{-/-} MEFs compared to those in wild type (WT) cells (Fig. 1a). Accordingly, we observed
91 increased amounts of secreted IFN-β protein in culture supernatants from *Stim1*^{-/-} MEFs (Fig. 1b).
92 Due to the well-established role of STIM1 in SOCE, it was possible that the increased type I IFN
93 response in *Stim1*^{-/-} MEFs was due to altered intracellular Ca²⁺ homeostasis. To check this possibility,
94 we compared responses between *Stim1*^{-/-} and *Orai1*^{-/-} MEFs, both of which show loss of SOCE (Fig.
95 1c). However, we did not observe enhanced *Ifnb1* expression in *Orai1*^{-/-} MEFs, indicating that block of
96 SOCE or altered intracellular Ca²⁺ levels do not contribute to increased type I IFN response observed
97 in *Stim1*^{-/-} MEFs.

98 To verify these observations in primary cells, we examined bone marrow-derived
99 macrophages (BMDMs) from WT (*Stim1*^{fl/fl}) and *Stim1*^{fl/fl}UBC-ERT2-cre mice to induce acute loss of
100 STIM1 expression after tamoxifen treatment (Fig. 1d). Similar to MEFs, we observed enhanced
101 expression of *Ifnb1* and *Il6* transcripts in *Stim1*^{-/-} BMDMs. Next, we examined if this enhanced type I
102 IFN expression phenotype was conserved in human macrophages. We generated *STIM1*^{-/-} THP1
103 cells by CRISPR/Cas9-mediated genome editing using two different gRNA sequences
104 (Supplementary Fig. 1). Similar to murine cells, we observed an induction of *IFNB1* and *IL6* mRNAs
105 and increased IFN-β secretion in *STIM1*^{-/-} THP1 clones (Fig. 1e, f). Moreover, exogenous expression
106 of STIM1 in these THP1 clones significantly rescued the phenotype by decreasing type I IFN
107 expression. Taken together, these data strongly demonstrate an inhibitory role of STIM1 in type I IFN

108 responses. STIM2 is another member of the STIM family that shares 66% amino acid sequence
109 similarity with STIM1¹⁶. Both of them are ER-resident proteins, but they function differently in sensing
110 depletion of the ER Ca²⁺ stores and efficacy to activate Orai channels. STIM1 plays a dominant role in
111 activation of SOCE while STIM2 is involved in ER Ca²⁺ homeostasis by sensing subtle changes in
112 [Ca²⁺]_{ER}^{22 23}. To check a possible function of STIM2 in regulation of type I IFN responses, we
113 generated two independent *STIM2*^{-/-} THP1 clones. However, neither of the STIM2 KO clones showed
114 elevated expression of *IFNB1* transcripts (Supplementary Fig. 2). Collectively, these results establish
115 a specific role for STIM1 in regulating the resting state of the type I IFN responses in murine and
116 human cells.

117

118 **STING-TBK1-IRF3 pathway links perturbation in STIM1 expression to IFN-β expression**

119 Since both STIM1 and STING, an important regulator for the type I IFN responses, localize to the ER
120 membrane, we checked the possibility that STIM1 regulates the function of STING. Upon activation of
121 STING via exposure to its ligand 2',3'-cGAMP, we observed a pronounced enhancement of *Irfb1*
122 transcript and protein levels in *Stim1*^{-/-}, but not *Orai1*^{-/-} MEFs when compared to those in WT MEFs
123 (Fig. 2a). This higher type I IFN response in *Stim1*^{-/-} MEFs was also observed in the presence of
124 cytosolic DNAs after transfection with IFN stimulatory DNA (ISD) or poly(dA:dT) that are known to
125 activate the STING pathway, but not with poly(I:C), a poor agonist of the STING pathway (Fig. 2b,
126 left). Similarly, we observed elevated transcripts of *IFNB1* in *STIM1*^{-/-} THP1 cells transfected with
127 2',3'-cGAMP, but not poly(I:C) (Fig. 2b, right).

128 To determine whether deficiency of STIM1 induces an increase in type I IFN response through
129 the STING-TBK1-IRF3 pathway, we checked for activated IRF3 and TBK1 in WT and *Stim1*^{-/-} MEFs.
130 We examined localization of GFP-IRF3, which was exclusively in the cytoplasm in WT MEFs but
131 showed almost equal distribution in the cytoplasm and nuclei in *Stim1*^{-/-} MEFs (Fig. 2c).
132 Biochemically, we detected enhanced homo-dimers of IRF3, in *Stim1*^{-/-} MEFs compared to WT cells
133 under resting conditions (Fig. 2d). Furthermore, we found enhanced levels of phosphorylated TBK1

134 and accordingly increased ratio of p-TBK1 vs. total TBK1 in *Stim1*^{-/-} MEFs, BMDMs and *STIM1*^{-/-}
135 THP1 cells (Fig. 2e). We could also detect enhanced dimerization of endogenous STING in *Stim1*^{-/-}
136 MEFs, which is considered an active form of STING (Supplementary Fig. 3a). Likewise, *STIM1*^{-/-}
137 HEK293T cells stably expressing STING also showed enhanced STING dimers and multimers
138 (Supplementary Fig. 3b). Next, we examined whether co-deletion of STING in STIM1-deficient cells
139 could rescue this enhanced IFN-β expression phenotype. Deletion of both *Stim1* and *Tmem173* (gene
140 encoding STING) in MEFs (double knockout, DKO) dramatically reduced *Irfnb1* and *Il6* transcripts
141 under resting or cGAMP-treated conditions (Fig. 2f). Co-deletion of *Tmem173* also rescued increased
142 IFN-β secretion observed in *Stim1*^{-/-} MEFs treated with poly (dA:dT) (Fig. 2g). We observed very
143 similar results using THP1 cells. Deletion of both *STIM1* and *TMEM173* in double knockout (DKO)
144 THP1 cells was confirmed by immunoblotting and SOCE measurements (Fig. 2h). DKO THP1 cells
145 showed reduced *IFNB1* and *IL6* mRNA levels, suggesting that the elevated cytokine expression in
146 *STIM1*^{-/-} THP1 cells were derived from increased STING activity. Together, these results suggest that
147 the increase in type I IFN responses observed in STIM1-deficient cells is mediated by the STING-
148 TBK1-IRF3 pathway, and STIM1 plays a novel role in type I IFN signaling via regulating STING
149 function.

151 **Increased type I IFN responses in patient lacking STIM1 expression**

152 Previously, patients showing SCID symptoms and bearing homozygous nonsense mutation of STIM1
153 (E136X) were shown to lack STIM1 expression due to nonsense-mediated mRNA decay²⁴. To mimic
154 the phenotype of this patient, we transduced STIM1-deficient cells with viral vectors encoding WT and
155 *STIM1*^{E136X} proteins. We confirmed lack of STIM1 expression in *Stim1*^{-/-} MEFs transduced to express
156 *STIM1*^{E136X} while those with *STIM1*^{WT} showed expression similar to the endogenous protein in WT
157 MEFs (Fig. 3a). Importantly, expression of *STIM1*^{WT} but not *STIM1*^{E136X} rescued the increased type I
158 IFN response in *Stim1*^{-/-} MEFs (Fig. 3b).

159 To examine if this was true in STIM1-deficient patients, we harvested primary cells from a
160 patient lacking STIM1 expression due to a homozygous *STIM1* mutation c.478del, p.(Ser160fs). The
161 lack of STIM1 expression in patient's PBMCs was confirmed by immunoblotting (Fig. 3c). Patient
162 serum showed enhanced IFN- β , IL-6 and TNF cytokines when compared to those observed in three
163 healthy controls (Fig. 3d). Consistently, we also observed enhanced expression of ISGs in PBMCs
164 and monocytes from the patient, when compared to those in two healthy controls (Fig. 3e).
165 Interestingly, the patient also exhibited very mild SAVI-like symptoms – he suffered from
166 desquamation and blistering with skin eruptions mainly affecting the palm, soles of the feet and
167 cheeks. He also showed pronounced nail dystrophy²⁵. Together, these data confirm that loss of
168 STIM1 in humans enhances expression of type I IFN, proinflammatory cytokines and ISGs, similar to
169 murine cells.

170

171 **STIM1 interacts with STING for its retention at the endoplasmic reticulum**

172 The increased type I IFN response together with higher basal activity of the STING-TBK1-IRF3
173 pathway in STIM1-deficient cells suggests that STIM1 may be involved in maintaining the resting state
174 of the STING pathway. Microscopy analysis showed a strong co-localization between STIM1 and
175 STING in the ER (Fig. 4a). Hence, we checked if STIM1 can physically interact with STING to retain it
176 in the ER. When co-expressed in HEK293T cells, STIM1 was specifically identified from
177 immunoprecipitates of STING (Fig. 4b). In addition, we also validated association between
178 endogenous STIM1 and STING proteins by immunoprecipitation (Fig. 4c). This association was
179 specific because another ER-resident protein, calnexin could not be detected in immunoprecipitates of
180 STIM1.

181 Next, we examined association between STIM1 and STING upon activation of either of the
182 proteins. We activated STIM1 by treatment with thapsigargin that depletes the ER Ca²⁺ stores, and
183 activated STING using its ligand, 2',3'-cGAMP. We observed reduced biochemical association
184 between the two proteins by stimulation of either STIM1 or STING (Fig. 4d). These data indicate that

185 STING and STIM1 form a protein complex that is dissociated due to conformational changes induced
186 by stimulation of either of these proteins. Association between STING and STIM1 prompted us to
187 check for a possible role of STING in regulating the function of STIM1. We observed reduced SOCE
188 induced by thapsigargin or anti-CD3 antibody treatment in HEK293T and Jurkat T cells
189 overexpressing STING (Supplementary Fig. 4a, b, c). In addition, we observed enhanced STIM1
190 translocation to the ER-PM junctions in thapsigargin treated STING-deficient (*Tmem173*^{-/-}) MEFs
191 (Supplementary Fig. 4d). Conversely, there was significant enhancement of SOCE in *TMEM173*^{-/-}
192 Jurkat cells (Supplementary Fig. 4e, f). This enhancement was not observed in THP1 cells, indicating
193 cell type specificity (Fig. 2h). Taken together, these data show that association with STING impacts
194 the function of STIM1 in mediating SOCE.

195 STING contains four transmembrane (TM) segments in its N terminus that span the ER
196 membrane (Fig. 4e)¹. STING N-terminal domain (NTD) containing the TM segments plays an
197 important role in its ER localization, trafficking and interaction with regulators including ZDHHC1,
198 AMFR, TRIM32, and RNF5^{26, 27, 28, 29}. Tumor DNA viral proteins, E1A and E7 also bind to STING NTD
199 to inhibit downstream signaling²⁸. The cytoplasmic region (C-terminal domain, CTD) of STING
200 contains the dimerization domain (DD), CDN-binding region, and the C-terminal tail (CTT) that
201 interacts with TBK1 and IRF3. STIM1 has an N-terminal ER-luminal region containing the Ca²⁺-
202 sensing EF-hand motifs and sterile alpha motif (SAM) domain that is important for its multimerization
203 after ER Ca²⁺ depletion. It also has a single TM domain that traverses the ER membrane. The
204 cytoplasmic C terminus contains multiple functional domains including coiled-coil domains (CC) 1,
205 CC2, CC3, a serine/threonine-rich domain (S/T), and a lysine-rich domain (poly-K) that are important
206 for binding to the plasma membrane after depletion of ER Ca²⁺ stores. A fragment containing CC2
207 and CC3 of STIM1 called the CRAC activation domain (CAD) or the STIM1 Orai activating region
208 (SOAR) was identified to interact directly with Orai1 subunits to gate them^{16, 29}.

209 To determine their interaction domains, we carried out co-immunoprecipitation using lysates of
210 HEK293T cells overexpressing full-length, NTD or CTD of STING together with full-length STIM1.

211 These results showed NTD of STING as a major STIM1-interacting domain while its CTD interacted
212 weakly with STIM1 (Fig. 4f, left panels). To uncover the domain(s) of STIM1 involved in interaction
213 with STING, we performed GST pull-down experiments by incubating bacterially purified GST-fused
214 fragments of STIM1 with lysates of HEK293T cells overexpressing full-length, NTD or CTD of STING.
215 From this analysis, we identified a predominant interaction between the N terminus of STIM1
216 containing the TM segment (a.a. 1-249) and STING NTD, and a weaker binding of the cytoplasmic
217 fragment predominantly containing the S/T-rich region of STIM1 to STING CTD (Fig. 4f, right panels).
218 These data suggest that interaction between STIM1 and STING is predominantly mediated by their
219 TM domains on the ER membrane with weak additional interactions between their cytoplasmic
220 regions.

221

222 **STIM1 acts as an ER retention factor to suppress the activity of STING**

223 Ligand binding induces conformational rearrangement and trafficking of STING from the ER to the
224 ERGIC and the Golgi apparatus^{14, 30, 31}. Since STIM1 interacted strongly with STING NTD, which is
225 crucial for STING localization, we hypothesized that STIM1 may control the ER localization of STING.
226 To validate this hypothesis, we examined the localization of STING in WT and *Stim1*^{-/-} MEFs by co-
227 staining with ERGIC marker (ERGIC-53/p58). We observed a significant population of *Stim1*^{-/-} MEFs
228 showing partial localization of STING at the ERGIC without any stimulation, and this population
229 increased much faster in *Stim1*^{-/-} MEFs infected with the DNA virus, herpes simplex virus type-1
230 (HSV-1) when compared to WT MEFs (Fig. 5a). To check how interaction with STIM1 influences the
231 function of STING, we monitored the translocation kinetics of STING after treatment of WT or *Stim1*^{-/-}
232 MEFs with 2',3'-cGAMP and observed faster translocation of STING into the ERGIC in *Stim1*^{-/-} MEFs
233 than in WT cells (Fig. 5b). Together with our biochemical analysis, these data suggest that STIM1
234 physically interacts with STING to promote its retention onto the ER membrane.

235 We checked if overexpression of STIM1 can inhibit the function of STING using *Irfnb* promoter-
236 driven luciferase reporter (IFN-Luc) assays after 2',3'-cGAMP treatment. In cells co-expressing STING

237 and increasing amounts of full length or the N- and C-terminal binding fragments of STIM1, we
238 observed a dose-dependent inhibition of luciferase reporter expression (Fig. 5c). In support of our
239 biochemical analyses, the N-terminal TM-containing fragment of STIM1 (a.a. 1-249) showed a
240 stronger inhibition of luciferase reporter activity than the cytoplasmic domain (a.a. 400-600) while
241 STIM1 fragments (a.a. 250-400 and a.a. 600-685) that do not interact with STING did not affect
242 luciferase activity. Of note, expression of full-length STIM1 or its N-terminal fragment (a.a. 1-249) did
243 not influence the luciferase activity when stimulated with poly(I:C). These data validate functional
244 interaction between STIM1 and STING proteins.

245 The genetic lesions of patients exhibiting autoinflammatory vasculopathy and autoimmunity
246 were mapped to single amino acid substitutions in STING¹¹. These substitution mutations changed
247 one of the conserved residues V147, N154, or V155, all of which are localized in or around the STING
248 dimerization domain³². In addition, these substitutions lead to localization of STING at the ERGIC and
249 constitutive TBK1 and IRF3 activation and uncontrolled type I IFN response^{11, 13}. We examined if
250 these disease-associated STING mutants retained binding to STIM1. Using immunoprecipitation
251 analysis, we observed reduced interaction of the STING SAVI mutants with STIM1 and
252 overexpression of full-length or N-terminal fragment of STIM1 could suppress *Irf3* promoter-driven
253 luciferase activity of these mutants. (Supplementary Fig. 5a, b). In support of these data, confocal
254 analyses showed a partial block of constitutive ERGIC localization of these mutants in the presence of
255 STIM1 (Supplementary Fig. 5c). Collectively, these results confirm the previous observations that exit
256 from the ER is an important step for the activation of STING and STIM1 can block this trafficking via
257 direct interaction.

258

259 **Genetic inhibition of STIM1 expression primes antiviral activity**

260 We sought to determine whether deficiency of STIM1 influences activation of the type I IFNs in
261 response to DNA virus infection. To examine this, WT and *Stim1*^{-/-} MEFs were infected with DNA
262 viruses (e.g., HSV-1 and murine γ -herpesvirus, MHV-68). Spontaneous induction of IFN- β observed in

263 *Stim1*^{-/-} MEFs was substantially increased after HSV-1 infection (Fig. 6a). We also observed a
264 marked reduction in expression of GFP, encoded from the viral genome which served as an indicator
265 for viral replication in *Stim1*^{-/-} MEFs. We observed similar results using another DNA virus, MHV-68.
266 Similar to HSV-1 infection, MHV-68-infected *Stim1*^{-/-} MEFs showed much lower expression of the
267 viral genome-driven GFP, as well as early and late phase viral transcripts (e.g., *ORF57* and *ORF29*,
268 respectively), indicative of a lower viral burden (Fig. 6b). In consistence with these data, *Stim1*^{-/-}
269 MEFs showed enhanced phosphorylation of IRF3 upon HSV-1 infection (Fig. 6c). We observed
270 similar results in primary cells, where *Stim1*^{-/-} BMDMs showed enhanced expression of *Irfn1* and *Irf6*
271 mRNAs under resting conditions, as well as after HSV-1 infection (Fig. 6d). Together, these data
272 show that loss of STIM1 increases resistance to DNA virus infections.

273 Next, we validated these observations in *STIM1*^{-/-} THP1 macrophages. Similar to data with
274 mouse cells, STIM1 deficiency rendered human macrophages resistant to HSV-1, decreasing
275 expression of GFP as observed by microscopy and transcript analyses (Fig. 6e). Accordingly, we
276 observed enhanced expression of *IFNB1* transcripts in *STIM1*^{-/-} THP1 cells. Previously, it was shown
277 that anti-viral immunity against HIV infection also relies on the cGAS-STING pathway due to the
278 presence of cytosolic DNA generated by reverse-transcription^{8, 33}. To investigate whether STIM1
279 deletion imparts resistance to HIV, we infected wild type and *STIM1*^{-/-} THP1 cells with GFP-HIV and
280 observed a dramatic reduction of HIV infection in *STIM1*^{-/-} THP1 cells as judged by frequency of
281 GFP⁺ cells (Fig. 6f). Together, these results suggest that deficiency of STIM1 can prime host
282 response against infection with DNA viruses and retroviruses in various murine and human cell types.

283 Many DNA viruses, including HSV-1 are known to activate Ca²⁺ signaling for a productive
284 infection³⁴. Hence it is possible that resistance to DNA virus infection in *Stim1*^{-/-} MEFs may be due to
285 loss of SOCE. To determine the contribution of SOCE versus enhanced STING activity in host
286 resistance to DNA virus infection, we compared responses of *Stim1*^{-/-} and *Orai1*^{-/-} MEFs to HSV-1
287 infection. We observed a moderate resistance to HSV-1 infection in *Orai1*^{-/-} MEFs, but in comparison,
288 the resistance to HSV-1 infection was approximately 100-fold more pronounced in *Stim1*^{-/-} cells

289 (Supplementary Fig. 6a). In support of the SOCE-independent role of STIM1 in regulation of STING
290 function, we found that *Ifnb1* mRNA expression was not increased after HSV-1 infection in *Orai1*^{-/-}
291 cells contrary to *Stim1*^{-/-} cells. Finally, *Stim1*^{-/-} MEFs when treated with inhibitor of the IFN receptor-
292 JAK-STAT pathway, tofacitinib, became susceptible to HSV-1 infection (Supplementary Fig. 6b).
293 Together, these results indicate a predominant role of the type I IFN pathway in the resistance of
294 STIM1-deficient cells to viral infections.

295

296 **Ablation of STIM1 primes type I IFN response in vivo**

297 To gain insight into the importance of STIM1 in host defense against viral infection in vivo, we
298 investigated the antiviral immune response in *Stim1*^{fl/fl} and *Stim1*^{fl/fl}*Lyz2*-cre mice. In parallel, to
299 compare the contribution of SOCE in host resistance to viral infections, we generated conditionally
300 targeted *Orai1* animals (Supplementary Fig. 7a), which were bred with *Lyz2*-cre for two generations.
301 BMDMs differentiated from bone marrows of *Orai1*^{fl/fl}*Lyz2*-cre animals showed almost a complete loss
302 of *Orai1* transcripts and SOCE (Supplementary Fig. 7b, c). Since HSV-1 is a neurotropic virus and the
303 leading cause of sporadic viral encephalitis, we investigated the effects of *Orai1* and *Stim1* deficiency
304 on HSV-1-induced lethality and viral loads in the brain. When infected with HSV-1 intravenously,
305 control (*Stim1*^{fl/fl} and *Orai1*^{fl/fl}) as well as *Orai1*^{fl/fl}*Lyz2*-cre animals showed susceptibility and died
306 within 6-8 days of infection (Fig. 7a, b). In contrast *Stim1*^{fl/fl}*Lyz2*-cre mice were completely resistant to
307 HSV-1-induced lethality, and accordingly, recovered from loss of body weight. Viral titers in the brains
308 obtained from *Stim1*^{fl/fl}*Lyz2*-cre mice were significantly lower than *Stim1*^{fl/fl} animals (Fig. 7c).
309 Importantly, serum cytokine measurements showed elevated levels of serum IFN-β, IL-6 and TNF in
310 uninfected as well as HSV-1-infected *Stim1*^{fl/fl}*Lyz2*-cre mice, when compared to littermate controls
311 (Fig. 7d). Taken together, our data indicate that genetic deletion of *Stim1* but not *Orai1* can impart
312 protection from HSV-induced encephalitis and lethality, due to pre-activation of the STING-mediated
313 type I IFN signaling pathway.

314

315 Discussion

316 STING and STIM1 commonly contain transmembrane domain(s) in their N termini and predominantly
317 localize to the ER membrane. Co-immunoprecipitation experiments showed an association between
318 the two proteins, that was primarily mediated by their N-terminal transmembrane domains. We
319 showed that loss of STIM1 renders cells and mice strongly resistant to viral infections due to
320 enhanced expression of type I IFNs and pro-inflammatory cytokines. Importantly, a patient with a
321 mutation in *STIM1* that abrogated STIM1 expression also showed elevated cytokines and ISGs.
322 Furthermore, some of the patient's clinical features, principally the skin and nail manifestations
323 resemble that of SAVI patients, suggesting that the excessive type I IFNs do have adverse biological
324 manifestation in this condition²⁵. Mechanistically, enhanced translocation and dimerization of STING
325 by STIM1 deficiency suggest that STIM1 may preferentially bind to STING monomers at the ER to
326 prevent its spontaneous activation. Conversely, we also found that STING deficiency augmented
327 translocation of STIM1 and Ca²⁺ entry triggered by depletion of ER Ca²⁺ stores. Therefore, our studies
328 suggest that physical and functional association between STIM1 and STING is crucial for
329 maintenance of the resting state of both pathways.

330 We showed that enhanced type I IFN expression in STIM1-deficient cells is not mediated by
331 Ca²⁺ signaling by comparative studies with *Orai1*-deficient cells and animals. STIM1 deficiency made
332 cells and mice strongly resistant to HSV-1 infections. Since many viruses including HSV-1³⁴, require
333 elevated Ca²⁺ levels for their replication, we determined the contribution of the Ca²⁺-dependent (i.e.,
334 decreased SOCE) vs. Ca²⁺-independent mechanisms (i.e., enhanced type I IFN response) involved in
335 anti-viral immunity in STIM1-deficient cells using two independent molecular tools, *Orai1*^{-/-} cells/mice
336 and JAK inhibitors. These results suggest that decreased viral burden in STIM1-deficient cells and
337 mice is predominantly derived from enhanced type I IFN responses. Whether the same principle can
338 be applied to other viruses with various degrees of dependence on Ca²⁺ signaling and activation of
339 the STING pathway needs further studies.

340 Although much is understood regarding the mechanisms underlying activation of STING
341 including ligand binding, trafficking and interaction with downstream effector molecules, little is known
342 about regulation of its resting state. Multiple mechanisms underlying STING inhibition have been
343 uncovered due to the importance of timely inactivation of the type I IFN signaling pathway. NLRX1
344 and ATG9a have been shown to inhibit STING-TBK1 interaction^{26, 27}. In addition, K48-linked
345 polyubiquitination by RNF5 and TRIM30a results in STING degradation after ligand binding^{35, 36}. All
346 these inhibitory mechanisms target STING function after ligand binding and trafficking. However,
347 inhibition of STING trafficking by brefeldin A, an inhibitor of ADP ribosylation factor (ARF) GTPases,
348 blocks activation of the downstream pathway, suggesting that trafficking of STING is crucial for its
349 function¹⁴. Consistently, our studies reveal a novel mechanism of regulation of STING activity,
350 inhibition of STING trafficking via direct interaction with STIM1. Activity of three of the disease-
351 associated STING variants; V147L, N154S, and V155M was suppressed by STIM1 in part via
352 blocking their translocation to the ERGIC, demonstrating a therapeutic potential of our finding. In
353 summary, our study identifies STIM1 as an “ER retention factor” to maintain ER residency and
354 inactive conformation of STING. Further, it suggests that one of the primary functions of CDN binding
355 to STING is to disrupt its association with STIM1 that would allow exit of STING from the ER. Further
356 dissection of the mechanisms underlying maintenance of the resting state of STING may inform the
357 design of specific therapeutic strategies geared towards enhancement/inhibition of STING activity in
358 the context of vaccination and sterile inflammatory diseases (e.g., AGS and SAVI), respectively.

359

360 **ACKNOWLEDGEMENTS**

361 We thank S. Bensinger (UCLA) for sharing THP1 cells, X. Liu and S. Smale (UCLA) for BMDM
362 differentiation protocols and reagents. We thank N-H. Park, K-H. Shin, M. K. Kang, R. Kim, Y. Wang
363 and T. M. Vondriska for sharing their confocal imaging facilities. We thank J-L. Casanova (Rockefeller
364 University) for providing STIM1 patient B cell line. This work was supported by the National Institute of
365 Health grants AI083432 and DE028432 (Y.G.) and AI130653 (S.S.). This work was also supported in

366 part by CA180779, CA200422, AI073099, AI116585, AI129496, AI140705, DE023926, DE027888,
367 Fletcher Jones Foundation, and Whittier Foundation (J.U.J).

368

369 **AUTHOR CONTRIBUTIONS**

370 Y.G. and S.S. designed research; S.S. performed all the in vitro experiments using MEFs, THP1 and
371 BMDMs with technical help from J.L.; J.S.W. performed biochemical experiments of interaction
372 between STIM1 and STING, SAVI mutant analyses, and in vivo HSV infection experiments with help
373 from B.W.; Y.M. E.-S, L.R and S.Savic collected and analyzed patient samples together with S.S and
374 J.S.W.; K.C. and D.S.A. performed the HIV infection experiments; G.J.S. and J.U.J. provided reagents
375 and protocols for in vitro HSV infections; G.C. helped with statistical analysis; C. R. and E.C. provided
376 reagents and protocols for in vivo HSV infections; T.T.W. and R.S. provided reagents and protocols
377 for MHV-68 infections; S.S. and Y.G. wrote the manuscript with input from all authors and supervised
378 the project.

379

380 **COMPETING INTERESTS**

381 The authors do not have any competing financial interests.

382

383

384 **References**

385

- 386 1. Ishikawa, H. & Barber, G.N. STING is an endoplasmic reticulum adaptor that facilitates innate
387 immune signalling. *Nature* **455**, 674-678 (2008).
- 388 2. Zhong, B. *et al.* The adaptor protein MITA links virus-sensing receptors to IRF3 transcription
389 factor activation. *Immunity* **29**, 538-550 (2008).
- 390 3. Sun, W. *et al.* ERIS, an endoplasmic reticulum IFN stimulator, activates innate immune
391 signaling through dimerization. *Proc Natl Acad Sci U S A* **106**, 8653-8658 (2009).

394

- 395 4. Barber, G.N. STING: infection, inflammation and cancer. *Nat Rev Immunol* **15**, 760-770
396 (2015).
- 397
398 5. Chen, Q., Sun, L. & Chen, Z.J. Regulation and function of the cGAS-STING pathway of
399 cytosolic DNA sensing. *Nat Immunol* **17**, 1142-1149 (2016).
- 400
401 6. Li, T. & Chen, Z.J. The cGAS-cGAMP-STING pathway connects DNA damage to
402 inflammation, senescence, and cancer. *J Exp Med* (2018).
- 403
404 7. Li, Y., Wilson, H.L. & Kiss-Toth, E. Regulating STING in health and disease. *J Inflamm (Lond)*
405 **14**, 11 (2017).
- 406
407 8. Yan, N., Regalado-Magdos, A.D., Stiggelbout, B., Lee-Kirsch, M.A. & Lieberman, J. The
408 cytosolic exonuclease TREX1 inhibits the innate immune response to human
409 immunodeficiency virus type 1. *Nat Immunol* **11**, 1005-1013 (2010).
- 410
411 9. Ahn, J., Gutman, D., Saijo, S. & Barber, G.N. STING manifests self DNA-dependent
412 inflammatory disease. *Proc Natl Acad Sci U S A* **109**, 19386-19391 (2012).
- 413
414 10. Crow, Y.J. & Manel, N. Aicardi-Goutieres syndrome and the type I interferonopathies. *Nat Rev*
415 *Immunol* **15**, 429-440 (2015).
- 416
417 11. Liu, Y. *et al.* Activated STING in a vascular and pulmonary syndrome. *N Engl J Med* **371**, 507-
418 518 (2014).
- 419
420 12. Melki, I. *et al.* Disease-associated mutations identify a novel region in human STING
421 necessary for the control of type I interferon signaling. *J Allergy Clin Immunol* **140**, 543-552
422 e545 (2017).
- 423
424 13. Jeremiah, N. *et al.* Inherited STING-activating mutation underlies a familial inflammatory
425 syndrome with lupus-like manifestations. *J Clin Invest* **124**, 5516-5520 (2014).
- 426
427 14. Dobbs, N. *et al.* STING Activation by Translocation from the ER Is Associated with Infection
428 and Autoinflammatory Disease. *Cell Host Microbe* **18**, 157-168 (2015).
- 429
430 15. Zhang, X. *et al.* Cyclic GMP-AMP containing mixed phosphodiester linkages is an endogenous
431 high-affinity ligand for STING. *Mol Cell* **51**, 226-235 (2013).
- 432
433 16. Prakriya, M. & Lewis, R.S. Store-Operated Calcium Channels. *Physiol Rev* **95**, 1383-1436
434 (2015).
- 435
436 17. Feske, S., Skolnik, E.Y. & Prakriya, M. Ion channels and transporters in lymphocyte function
437 and immunity. *Nat Rev Immunol* **12**, 532-547 (2012).

- 438
439 18. Baba, Y. & Kurosaki, T. Role of Calcium Signaling in B Cell Activation and Biology. *Curr Top*
440 *Microbiol Immunol* **393**, 143-174 (2016).
- 441
442 19. Srikanth, S., Woo, J.S., Sun, Z. & Gwack, Y. Immunological Disorders: Regulation of Ca(2+)
443 Signaling in T Lymphocytes. *Adv Exp Med Biol* **993**, 397-424 (2017).
- 444
445 20. Lacruz, R.S. & Feske, S. Diseases caused by mutations in ORAI1 and STIM1. *Ann N Y Acad*
446 *Sci* **1356**, 45-79 (2015).
- 447
448 21. Notarangelo, L.D., Kim, M.S., Walter, J.E. & Lee, Y.N. Human RAG mutations: biochemistry
449 and clinical implications. *Nat Rev Immunol* **16**, 234-246 (2016).
- 450
451 22. Brandman, O., Liou, J., Park, W.S. & Meyer, T. STIM2 is a feedback regulator that stabilizes
452 basal cytosolic and endoplasmic reticulum Ca²⁺ levels. *Cell* **131**, 1327-1339 (2007).
- 453
454 23. Soboloff, J., Rothberg, B.S., Madesh, M. & Gill, D.L. STIM proteins: dynamic calcium signal
455 transducers. *Nat Rev Mol Cell Biol* **13**, 549-565 (2012).
- 456
457 24. Picard, C. *et al.* STIM1 mutation associated with a syndrome of immunodeficiency and
458 autoimmunity. *N Engl J Med* **360**, 1971-1980 (2009).
- 459
460 25. Rice, A. *et al.* A report of novel STIM1 deficiency and 6 year follow up of two previous cases
461 associated with mild immunological phenotype. *doi:10.31219/osf.io/4duxt* (2018).
- 462
463 26. Guo, H. *et al.* NLRX1 Sequesters STING to Negatively Regulate the Interferon Response,
464 Thereby Facilitating the Replication of HIV-1 and DNA Viruses. *Cell Host Microbe* **19**, 515-528
465 (2016).
- 466
467 27. Saitoh, T. *et al.* Atg9a controls dsDNA-driven dynamic translocation of STING and the innate
468 immune response. *Proc Natl Acad Sci U S A* **106**, 20842-20846 (2009).
- 469
470 28. Lau, L., Gray, E.E., Brunette, R.L. & Stetson, D.B. DNA tumor virus oncogenes antagonize the
471 cGAS-STING DNA-sensing pathway. *Science* **350**, 568-571 (2015).
- 472
473 29. Yuan, J.P. *et al.* SOAR and the polybasic STIM1 domains gate and regulate Orai channels.
474 *Nat Cell Biol* **11**, 337-343 (2009).
- 475
476 30. Ishikawa, H., Ma, Z. & Barber, G.N. STING regulates intracellular DNA-mediated, type I
477 interferon-dependent innate immunity. *Nature* **461**, 788-792 (2009).
- 478
479 31. Mukai, K. *et al.* Activation of STING requires palmitoylation at the Golgi. *Nat Commun* **7**,
480 11932 (2016).

- 481
482 32. Ouyang, S. *et al.* Structural analysis of the STING adaptor protein reveals a hydrophobic dimer
483 interface and mode of cyclic di-GMP binding. *Immunity* **36**, 1073-1086 (2012).
- 484
485 33. Gao, D. *et al.* Cyclic GMP-AMP synthase is an innate immune sensor of HIV and other
486 retroviruses. *Science* **341**, 903-906 (2013).
- 487
488 34. Cheshenko, N. *et al.* Herpes simplex virus triggers activation of calcium-signaling pathways. *J*
489 *Cell Biol* **163**, 283-293 (2003).
- 490
491 35. Zhong, B. *et al.* The ubiquitin ligase RNF5 regulates antiviral responses by mediating
492 degradation of the adaptor protein MITA. *Immunity* **30**, 397-407 (2009).
- 493
494 36. Wang, Y. *et al.* TRIM30alpha Is a Negative-Feedback Regulator of the Intracellular DNA and
495 DNA Virus-Triggered Response by Targeting STING. *PLoS Pathog* **11**, e1005012 (2015).
- 496
497
498
499
500

501 **Figure Legends**

502 **Figure 1. STIM1 deficiency spontaneously induces type I IFN response in murine and human**
503 **cells. a**, Representative immunoblot showing expression of STIM1 in wild type (WT) and *Stim1*^{-/-}
504 MEFs (left). qPCR analysis of indicated cytokines and ISGs in unstimulated indicated MEFs (right).
505 qPCR data show pooled technical replicates from two independent experiments (*Ifnb1* and *Il6*) and
506 one representative triplicate from two independent experiments (other genes). **b**, Levels of secreted
507 IFN- β from culture supernatants of unstimulated WT or *Stim1*^{-/-} MEFs. **c**, Representative traces
508 showing averaged SOCE from WT (31 cells), *Orai1*^{-/-} (30 cells) and *Stim1*^{-/-} (29 cells) MEFs after
509 passive depletion of intracellular Ca²⁺ stores with 1 μ M thapsigargin (TG) in the presence of external
510 solution containing 20 mM Ca²⁺ (left). Bar graph (middle) shows averaged baseline subtracted SOCE
511 (\pm s.e.m.) from four independent experiments. right: qPCR analysis of *Ifnb1* mRNA in indicated MEFs.
512 **d**, Representative immunoblot showing expression of STIM1 in BMDMs (left). qPCR analysis of *Ifnb1*
513 and *Il6* mRNA in unstimulated WT and *Stim1*^{-/-} BMDMs (right). **e**, Immunoblot showing expression of
514 STIM1 in wild type (WT) and *STIM1*^{-/-} THP1 cells generated using two independent sgRNAs (sg#2)
515 and 3 (sg#3). qPCR analysis of *IFNB1* and *IL6* mRNA in unstimulated WT, *STIM1*^{-/-} THP1 cells and
516 those reconstituted for expression of STIM1 (right two panels). **f**, Secreted IFN- β levels from culture
517 supernatants of untreated or PMA-differentiated WT or *STIM1*^{-/-} THP1 cells. Data show
518 representative triplicate from two independent experiments (panels **b**, **e** and **f**) or pooled technical
519 replicates from two (**c**) or three (**d**) independent experiments. All immunoblot data (panels **a**, **d** and **e**)
520 are representative of three independent experiments with similar results. Data are shown as mean \pm
521 s.e.m. *p < 0.005, and **p < 0.0005 (unpaired/two-tailed *t* test – a, b, d; One-way ANOVA – c; and
522 Two-way ANOVA – e).

523

524 **Figure 2. STING-TBK1-IRF3 pathway links loss of STIM1 expression to *Ifnb1* transcription. a**,
525 qPCR analysis of *Ifnb1* mRNA in indicated MEFs under resting conditions or after stimulation with
526 2',3'-cGAMP for 2 or 4 h (left). Numbers on top indicate average fold change relative to WT MEFs.

527 Secreted IFN- β levels from culture supernatants of indicated MEFs after stimulation with 2',3'-cGAMP
528 (right). Data show pooled technical replicates from two independent experiments (qPCR) or one
529 representative triplicate from two independent experiments (ELISA) with similar results. **b**, qPCR
530 analysis of *Irfb1* transcripts in indicated MEFs transfected with interferon stimulatory DNA (ISD),
531 poly(dA:dT) or poly (I:C) for indicated time (left). qPCR analysis of *IFNB1* mRNA from untreated or
532 indicated nucleic acid-transfected THP1 cells. **c**, Representative confocal images showing localization
533 of GFP-IRF3 in indicated MEFs. Bar graph below depicts quantification from indicated number of
534 cells. Scale bars, 5 μ m. **d**, Representative immunoblot for detection of IRF3 under non-reducing
535 conditions in DSP-crosslinked indicated MEFs, (left). Bar graph (right) shows densitometry analysis of
536 IRF3 ratio (dimer/monomer) from three independent experiments. **e**, Representative immunoblots
537 showing expression of phospho-TBK1 (P-TBK1), total TBK1, and β -actin from indicated cells.
538 Numbers below indicate normalized fold change in ratio of P-TBK1/total TBK1. **f**, Representative
539 immunoblots showing expression of STIM1 and STING in WT, *Stim1*^{-/-}, or *Stim1*^{-/-} and *Tmem173*^{-/-}
540 double knock out (DKO) MEFs (left). Expression of *Irfb1* and *Il6* transcripts in indicated MEFs under
541 resting conditions (left two panels) or 4 h after stimulation with 2',3'-cGAMP (right two panels). **g**,
542 Secreted IFN- β levels from culture supernatants of indicated MEFs after stimulation with indicated
543 nucleic acids. **h**, Representative immunoblots showing expression of STIM1 and STING in WT,
544 *STIM1*^{-/-}, *TMEM173*^{-/-} or *STIM1*^{-/-} and *TMEM173*^{-/-} double knock out (DKO) THP1 cells (left).
545 Representative traces of averaged SOCE from WT (33 cells), *STIM1*^{-/-}, (30 cells), *TMEM173*^{-/-} (31
546 cells) and DKO (31 cells) THP1 cells after passive depletion of intracellular Ca²⁺ stores with 1 μ M
547 thapsigargin (TG) in the presence of external solution containing 2 mM Ca²⁺ (middle). Bar graph
548 shows averaged baseline subtracted SOCE (\pm s.e.m.) from three independent experiments. Right
549 panels show qPCR analysis of *IFNB1* or *IL6* mRNA in indicated THP1 cells. Data show representative
550 triplicates from two independent experiments with similar results (**b**, **d**, **f**, **g** and **h**) unless indicated. All
551 immunoblots are representative of at least three independent experiments with similar results. Data
552 are shown as mean \pm s.e.m. *p < 0.05, **p < 0.005, ***p < 0.0005 [Two-way ANOVA – a (left panel);
553 unpaired/two-tailed *t* test – a (right panel), b; Chi-square test – c; and One-way ANOVA – d, f, g, h].

554 **Figure 3. STIM1 deficiency causes enhanced type I IFN response in patient cells. a,**
555 Representative immunoblot showing expression of STIM1 in WT, *Stim1*^{-/-} MEFs or those expressing
556 either WT STIM1 (+STIM1) or STIM1^{E136X} (+E136X) mutant. **b,** qPCR analysis of *Irfn1* and *Ii6* mRNA
557 in indicated MEFs under resting conditions or 2 h after stimulation with 2',3'-cGAMP. Data show
558 representative triplicate from two independent experiments. **c,** Representative immunoblot showing
559 expression of STIM1 and GAPDH in PBMCs isolated from a healthy control (HC) and patient (Pat.). **d,**
560 Levels of indicated cytokines in serum samples from healthy controls (three independent donors) and
561 STIM1-deficient patient. Data show one representative triplicate from two independent experiments
562 (n=9 for three HCs). **e,** Taqman qPCR analysis of indicated ISGs from peripheral blood mononuclear
563 cells (PBMCs, top) or purified monocytes (below) from two independent healthy controls and STIM1-
564 deficient patient. Patient data (normalized to those of healthy controls) are derived from two
565 independent experiments performed in duplicates. Data are shown as mean ± s.e.m. *p < 0.05, **p <
566 0.005, ***p < 0.0005 (One-way ANOVA – b; and unpaired/two-tailed *t* test – d, e).

567

568 **Figure 4. STIM1 interacts with STING for its retention in the endoplasmic reticulum. a,**
569 Representative confocal microscopy image of STING-GFP and STIM1 in a MEF cell. Scale bar, 5 μm,
570 Inset – 1 μm. Pearson's *r* = 0.67 ± 0.08 from 9 cells. **b,** FLAG-immunoprecipitates (IP) from lysates of
571 HEK293T cells overexpressing FLAG-tagged STING and His-tagged STIM1 were immunoblotted for
572 detection of STIM1. Arrow, monomeric STING or STIM1; *, STING multimers. **c,** Immunoprecipitates
573 of endogenous STING from HEK293 cells were immunoblotted for detection of indicated proteins. **d,**
574 FLAG-immunoprecipitates (IP) from lysates of HEK293T cells expressing FLAG-tagged STING and
575 His-tagged STIM1 with or without treatment with thapsigargin (1 μM, 10 min; left) or 2', 3'-cGAMP (1
576 μM, 30 min and further incubation in media for 1 h) were immunoblotted for detection of the indicated
577 proteins. Bar graphs show densitometry analysis of normalized fold changes (mean ± s.e.m.) in
578 STIM1 and STING band intensity from three (left) and four (right) independent experiments. **e,**
579 Schematic showing domain structure of STING and STIM1 as indicated in the text. Amino acid

580 residues of STING and STIM1 fragments used in this study are indicated. **f**, Left – FLAG-
581 immunoprecipitates (IP) from lysates of HEK293T cells expressing FLAG-tagged full-length STING
582 (FL), NTD (a.a. 1-140), and CTD (a.a. 140-379) were immunoblotted for detection of STIM1. Right –
583 Purified recombinant GST-fused indicated fragments of STIM1 incubated with lysates of HEK293T
584 cells expressing FLAG-tagged, FL, NTD or CTD of STING were immunoblotted with anti-FLAG
585 antibody. Immunoblots in panels **b**, **c**, and **f** are representative of four independent experiments. * $p <$
586 0.005 (unpaired/two-tailed t test - d).

587

588 **Figure 5. STIM1 inhibits STING trafficking to the ER-Golgi intermediate compartment. a,**
589 Representative confocal microscopy images of WT or *Stim1*^{-/-} MEFs stably expressing STING-GFP
590 under resting conditions (top two panels) or 4 h after HSV-1 infection (bottom 3 panels) and stained
591 for endogenous p58 (ERGIC). Scale bars, 10 μ m. Bar graph shows quantification of indicated number
592 of cells showing STING translocation to the ERGIC under resting conditions or after infection with
593 HSV-1 for indicated times. Data are derived from two independent experiments. **b**, Representative live
594 cell epifluorescence images of WT (top) or *Stim1*^{-/-} (bottom) MEFs after treatment with 1 μ M 2', 3'-
595 cGAMP for the indicated times showing translocation of STING-GFP into the ERGIC (left). Line graph
596 on the right shows normalized rate of translocation of STING in WT (9 cells) and *Stim1*^{-/-} (11 cells)
597 MEFs from two independent experiments. Scale bar, 10 μ m. **c**, Reporter assays for *Irfb1* promoter
598 activity in HEK293T cells transfected with STING and increasing amounts of full length STIM1 or its
599 indicated fragments, 6 hours after stimulation with 2', 3' cGAMP (top) or poly(I:C) (below). Data show
600 representative triplicate from two independent experiments. * $p <$ 0.005, ** $p <$ 0.0005 Chi square test
601 (a) and one-way ANOVA (c); N.S. – not significant.

602

603 **Figure 6. Ablation of STIM1 enhances host defense towards DNA viruses and HIV by priming**
604 **type I IFN responses. a**, qPCR analysis of *Irfb1* and GFP transcripts in uninfected or HSV-1-GFP-
605 infected (MOI 0.1, 24 h) WT or *Stim1*^{-/-} MEFs. Data show pooled technical replicates from two

606 independent experiments. **b**, qPCR analysis of GFP and indicated viral mRNAs in MHV-68-GFP-
607 infected (MOI 0.2, 24 h) WT or *Stim1*^{-/-} MEFs. Data show pooled technical replicates from three
608 independent experiments. **c**, Representative immunoblots showing expression of phospho-IRF3 (P-
609 IRF3), total IRF3, and β -actin from untreated or HSV-1-infected (MOI 5.0) WT or *Stim1*^{-/-} MEFs for
610 indicated time points. **d**, qPCR analysis of *Ifnb1* and *Il6* mRNA in untreated or HSV-1-GFP-infected
611 (indicated MOI, 24 h) WT or *Stim1*^{-/-} BMDMs. Data shows representative triplicate from two
612 independent experiments. **e**, Top two panels show representative GFP images in HSV-1-GFP-
613 infected (MOI 10, 24 h) WT, (left) and *STIM1*^{-/-} (right) THP-1 cells. Below: qPCR analysis of *IFNB1*
614 and GFP transcripts from the same cells. Scale bars, 10 μ m. Data shows representative triplicate from
615 two independent experiments. **f**, Representative flow plots showing frequency of HIV-GFP-infected
616 WT (left) or two different *STIM1*^{-/-} (right two panels) THP1 cell lines (MOI 2.0, 24 h). Bar graph shows
617 averaged frequency of HIV-GFP-positive indicated THP1 cell lines in the presence or absence of HIV
618 reverse transcriptase inhibitor azidothymidine (AZT, 5 μ M) from four independent experiments.
619 Immunoblots in panel **c** and epifluorescence images in panel **e** are representative of three and two
620 independent experiments respectively. *p < 0.005 and **p < 0.0005 [Two-way ANOVA – a (left panel),
621 d, e (right panel), f; unpaired/two-tailed *t* test – a (right panel), b; One-way ANOVA – e (left panel)].

622

623 **Figure 7. STIM1 deficiency enhances host defense against HSV-1 infection in vivo.** **a**, Kinetics of
624 survival (top) and body weight changes (bottom) of indicated numbers of control (*Stim1*^{fl/fl}) and STIM1-
625 deficient (*Stim1*^{fl/fl}*Lyz2-cre*) mice (6-7-week old) after intravenous injection with HSV-1 (1 x 10⁷ PFU
626 per mouse). **b**, Kinetics of survival (top) and body weight changes (bottom) of indicated numbers of
627 control (*Orai1*^{fl/fl}) and Orai1-deficient (*Orai1*^{fl/fl}*Lyz2-cre*) mice after intravenous injection with HSV-1 (1
628 x 10⁷ PFU per mouse). Mice that lost >20% body weight were euthanized. **c**, Virus load in control
629 (*Stim1*^{fl/fl}) and STIM1-deficient (*Stim1*^{fl/fl}*Lyz2-cre*) mouse brains 3 days after intravenous injection with
630 HSV-1. **d**, ELISA analyses of the indicated cytokines from the sera of control (*Stim1*^{fl/fl}) and *Stim1*-
631 deficient (*Stim1*^{fl/fl}*Lyz2-cre*) mice after intravenous injection with HSV-1 for indicated times. Data in

632 panels **a** and **b** are pooled from two independent experiments. Panels **c** and **d** show mean +/- s.e.m.
633 from indicated number of animals (each symbol represents data from individual animal). *p < 0.05, **p
634 < 0.005, ***p < 0.0005 (unpaired/two-tailed *t* test).

635

636

637

638 **Methods**

639 **Chemicals and Antibodies.** Fura 2-AM (F1221) was purchased from ThermoFisher Scientific.
640 Thapsigargin and ionomycin were purchased from EMD Millipore. Poly(I:C) (P1530) was purchased
641 from Millipore Sigma. Poly(dA:dT) (tlrl-patn) and 2',3'-cGAMP (tlrl-nacga23) were purchased from
642 InvivoGen. Tofacitinib (S500110MG) was purchased from Selleck Chemical LLC. Antibodies for
643 detection of STIM1 (5668S), phosphor-IRF3 (29047S), IRF3 (4302S), phosphor-TBK1 (5483S), total
644 TBK1 (3504S), STING (13647S), 6xHis tag (12698S), and STIM2 (4917S) were purchased from Cell
645 Signaling Technologies. Antibodies for detection of FLAG tag (F3040), p58 (ERGIC marker, E1031)
646 and human Orai1 (AB9868) were purchased from Millipore Sigma. Antibody for detection of β -actin
647 (sc-47778) was obtained from Santa Cruz Biotechnology and antibodies for detection of STIM1 (clone
648 5A2) and GAPDH (GTX100118) from human PBMCs were obtained from Sigma and GeneTex
649 respectively.

650 **Plasmids and cells.** STIM1-YFP plasmid has been described previously³⁷. Human STIM1 cDNA was
651 subcloned into a lentiviral vector, FGIF (kind gift from Dr. Dong Sun An, UCLA) with a C-terminal
652 FLAG tag and pcDNA 3.1 mychis plasmid. GST-tagged truncated fragments of STIM1 corresponding
653 to amino acids 1-249 (containing the EF-hand, SAM domain and transmembrane segment), 250–400
654 (containing coiled-coil domains 1 and 2), the CAD domain (amino acids 342–448), 400–600 (the
655 serine and threonine-rich region), and 600–685 (the C-terminal PIP₂-interacting domain) have been
656 previously described³⁷. Fragments of STING corresponding to the N-terminal TM domain (a.a. 1-154)
657 and C-terminal domain (a.a. 149-379), both tagged with a FLAG tag in the C-terminus, were
658 subcloned into pMSCV-CITE-eGFP-PGK-Puro vector. Full-length cDNA of human STING and SAVI
659 mutants corresponding to V147L, N154S and V155M were subcloned into pEGFPN1 vector to
660 generate a C-terminal GFP fusion protein and into pMSCV-CITE-eGFP-PGK-Puro vector that
661 encodes a C-terminal FLAG tag using primers described in Supplementary Table 1. Oligonucleotides
662 encoding sgRNAs to delete *STIM1*, *STIM2* and *STING* were subcloned into lentiGuide-Puro vector
663 (Addgene, #52963). HEK293T, Vero and Jurkat E6-1 T cell lines were obtained from American Type

664 Culture Collection center (ATCC, Manassas, VA). WT and *Stim1*^{-/-} MEFs were generated by breeding
665 *Stim1*^{fl/fl} mice (Jackson Laboratory, stock No. 023350) with *CMV-cre* mice (Jackson Laboratory, stock
666 No. 006054). MEFs were established using standard protocols from E14.5 embryos and retrovirally
667 transduced with SV40 large T antigen in a plasmid encoding hygromycin resistance for
668 immortalization. *Orai1*^{-/-} MEFs have been previously described³⁸.

669 **Cell Culture.** MEFs, Vero and HEK293T cells were grown in complete DMEM (Mediatech)
670 supplemented with 10% (v/v) fetal bovine serum (Hyclone), 2 mM L-glutamine (Mediatech), 10 mM
671 HEPES (Mediatech) and Penicillin/Streptomycin (Mediatech) at 37°C and 5% CO₂. BMDMs were
672 differentiated from bone marrow cells isolated from femur and tibia of 6-8-week-old mice. For
673 preparation of BMDMs, the bone marrow cells were cultured in 10% M-CSF-containing conditional
674 medium from HEK293T cells expressing recombinant M-CSF (a kind gift from Stephen Smale lab,
675 UCLA) for 4-6 days. BMDMs were cultured in the absence of M-CSF for at least 24 hours prior to
676 experimental use. THP1 and Jurkat T cells were cultured in RPMI (Mediatech) containing 10% fetal
677 bovine serum (Hyclone). Cells were infected with indicated MOIs of indicated viruses and harvested in
678 TRIzol Reagent for transcript expression analysis. For 2',3'-cGAMP treatment, MEFs or HEK293T
679 cells were treated with or without 1 μM 2',3'-cGAMP for 30 mins in digitonin permeabilization buffer
680 (50 mM HEPES, 100 mM KCl, 3 mM MgCl₂, 0.1 mM DTT, 85 mM sucrose, 0.2% BSA, 1 mM ATP, 0.1
681 mM GTP, pH 7.0) followed by culture medium for indicated times, after which the cells were harvested
682 for transcript analysis or reporter assays. MEFs were transfected with 5 μg of interferon stimulatory
683 DNA (ISD³⁹), polydA:dT or poly I:C using Lipofectamine 2000 (Thermofisher Scientific). For ELISAs,
684 MEFs were treated with cGAMP as described and supernatant harvested after 24 hrs.

685 **Mice.** *Stim1*^{fl/fl} animals were purchased from Jackson Laboratory (stock No. 023350) and bred with
686 *Lyz2-cre* animals (Jackson Laboratory, stock No. 004781) for two generations. Targeting of murine
687 *Orai1* was performed by flanking exon 2 with LoxP sites by homologous recombination in AB2.2
688 (129SvEv) embryonic stem (ES) cells. Exon 2 encodes for 201 a.a. out of a total of 304 a.a. of Orai1
689 protein. G418-resistant clones were screened by PCR for homologous recombination at both

690 homology arms. Chimeric mice with floxed *Orai1* alleles were generated by blastocyst injection of
691 heterozygous *Orai1^{fl/+}* ES cell clones. Founder *Orai1^{fl/+}* mice were bred with Flp-deleter mice (Jackson
692 Laboratory) to remove the neomycin resistance gene cassette. *Orai1^{fl/fl}* mice were backcrossed to
693 C57/BL6/J mice for at least 10 generations and then bred with *Lyz2-cre* mice to generate myeloid-
694 specific deletion of *Orai1*. All mice were maintained in pathogen-free barrier facilities and used in
695 accordance with protocols approved by the Institutional Animal Care and Use Committee at the
696 UCLA.

697 **Patient.** Sample collection from the patient was performed after obtaining written consent from his
698 parents according to the principles of the Declaration of Helsinki and after local ethics approval.
699 Detailed clinical evaluation was undertaken in appropriate clinical setting. PBMC isolation from
700 healthy control and patient human blood samples was performed by gradient separation using
701 Lymphoprep (Stem Cell Technologies). Monocytes were purified from PBMCs using a Monocytes
702 separation kit II (# 130-091-153, Miltenyi Biotec). The patient is a 4-year-old boy of consanguineous
703 Pakistani background, who initially presented to paediatric neurology due to poor mobility. A diagnosis
704 of STIM1 deficiency was made following referral to paediatric immunology due to recurrent
705 sinopulmonary infections. The patient has typical non-immunological features consistent with STIM1
706 deficiency including amelogenesis imperfecta resulting in complete dental clearance, anhidrosis and
707 muscle weakness. Surprisingly, the patient had mild immunodeficiency phenotype, with relatively
708 preserved immunological function, including appropriate responses to challenge vaccination²⁵.

709 **Virus amplification and concentration.** MHV68-GFP virus was amplified and titrated in NIH3T3
710 cells using standard protocols. HSV-1 KOS strain was used for all in vitro experiments and HSV-1 17+
711 strain was used for in vivo infection experiments. Both the strains were amplified and titrated in Vero
712 cells using standard protocols. HSV-1 17+ strain was concentrated for in vivo experiments. VSV-G
713 pseudotyped HIV-1_{NL4-3} strain-GFP reporter virus was amplified and titrated in HEK293T cells using
714 standard protocols.

715 **RNA isolation, cDNA synthesis and Real-time quantitative PCR.** Total RNA from cells harvested
716 in TRIzol Reagent (ThermoFisher) was isolated using the Direct-zol RNA isolation kit (Zymo
717 Research). RNA quantity and quality were confirmed with a NanoDrop ND-1000 spectrophotometer.
718 cDNA was synthesized using 2-3 μg of total RNA using oligo(dT) primers and Maxima Reverse
719 Transcriptase (ThermoFisher Scientific). Real-time quantitative PCR was performed using iTaq
720 Universal SYBR Green Supermix (Bio-Rad) and an iCycler IQ5 system (Bio-Rad) using gene-specific
721 primers described in Supplementary Table 1. Threshold cycles (C_T) for all the candidate genes were
722 normalized to those for *36b4* to obtain ΔC_T and further normalized to the values obtained for WT
723 samples to obtain $\Delta\Delta C_T$. The specificity of primers was examined by melt-curve analysis and agarose
724 gel electrophoresis of PCR products. Total RNA from human patient and healthy donors PBMCs and
725 monocytes harvested was isolated using the Total RNA purification Kit (Norgen Biotek Corp.). cDNA
726 was synthesized using 1-2 μg of total RNA using High-Capacity cDNA Reverse Transcription Kit
727 (ThermoFisher Scientific). Real-time quantitative PCR was performed using TaqMan Universal PCR
728 Master Mix (ThermoFisher Scientific) using FAM-MGB probes for detection of *MX1*
729 (Hs00895608_m1), *IFI44* (Hs00951349), *IFI44L* (Hs00915292_m1), *IFI27* (Hs01086370_m1), *ISG15*
730 (Hs00192713_m1), *CXCL10* (Hs01124251_g1), *RSAD2* (Hs01057264_m1), *IFIT1* (Hs01675197_m1),
731 *IFI6* (Hs00242571_m1), *OAS1* (Hs00973635_m1), *IL6* (Hs00985639_m1), and *HPRT1*
732 (Hs99999909_m1). The relative abundance of each transcript was normalized to the expression level
733 of *HPRT1* to obtain ΔC_T and further normalized to the values obtained for healthy controls to obtain
734 $\Delta\Delta C_T$.

735 **Cytokine measurement by ELISA.** ELISA was performed on cell culture supernatants from indicated
736 cells or serum samples harvested from mock or HSV-1-infected animals for detection of IFN β
737 (Biolegend, # 439407), IL-6 (ThermoFisher, # 88-7064-88) and TNF (ThermoFisher, # 88-7324-88).
738 Serum samples obtained from healthy controls or STIM1-deficient human patient were used for
739 detection of IFN β (PBL Assay Science, #41410), IL-6 (ThermoFisher Scientific, # 88-7066-22) and
740 TNF (ThermoFisher Scientific, # 88-7346-22).

741 **Single-cell Ca²⁺ imaging, live-cell epifluorescence or TIRF microscopy and confocal**
742 **microscopy.** THP1 and Jurkat T cells were loaded at 1 x 10⁶ cells/ml with 1 μM Fura 2-AM for 40 min
743 at 25°C and attached to poly-L-lysine-coated coverslips. MEFs or BMDMs were grown overnight on
744 coverslips and loaded with 1 μM Fura 2-AM for 40 min at 25°C for imaging. Intracellular [Ca²⁺]_i
745 measurements were performed using essentially the same methods as previously described⁴⁰. For
746 live-cell epifluorescence imaging of STING-GFP translocation kinetics, MEFs grown on coverslips
747 were perfused with Ringer's solution containing (in mM): 155 NaCl, 4.5 KCl, 2 CaCl₂, 1 MgCl₂, 10 D-
748 glucose, and 5 Na-HEPES (pH 7.4) and used for time course imaging. Cells were perfused with
749 digitonin permeabilization buffer (50 mM HEPES, 100 mM KCl, 3 mM MgCl₂, 0.1 mM DTT, 85 mM
750 sucrose, 0.2% BSA, 1 mM ATP, 0.1 mM GTP, pH 7.0) containing 1 μM 2',3'-cGAMP for 10 mins and
751 then the medium was replaced with Ringer's solution. For TIRF analysis of STIM1-YFP translocation,
752 MEFs were plated onto coverslip bottom dishes in medium and used for experiments. Medium was
753 replaced with Ringer's solution and cells were treated with 1 μM thapsigargin for passive depletion of
754 ER Ca²⁺ stores to monitor STIM1 translocation. TIRF microscopy was performed using an Olympus
755 IX2 illumination system mounted on an Olympus IX51 inverted microscope using previously described
756 methods³⁷. Acquisition and image analysis were performed using Slidebook (Intelligent Imaging
757 Innovations, Inc.) software and graphs were plotted using OriginPro8.5 (Originlab). For quantification
758 of TIRF intensity across different cells, individual regions of interest were selected and data were
759 analyzed as the ratio of fluorescence intensity at each time-point (F) to that at the start of the
760 experiment (F₀). For confocal analysis, uninfected or HSV-infected MEFs were fixed for 20 mins with
761 2.5% PFA at room temperature, permeabilized in buffer containing PBS + 0.2% Triton X-100, blocked
762 with same buffer containing 1% BSA and used for staining of ERGIC marker and confocal analysis.
763 Confocal laser scanning microscopy was performed using Fluoview FV10i Confocal Microscope
764 (Olympus), images were captured with a 60x oil objective. Images were processed for enhancement
765 of brightness or contrast using Fluoview software.

766 **Generation of STIM1, STIM2 and STING-deficient cells using CRISPR-Cas9 system.** To generate
767 lentiviruses for transduction, HEK293T cells were transfected with plasmid(s) encoding sgRNA and
768 packaging vectors (pMD2.G and psPAX2, Addgene) using calcium phosphate transfection method.
769 Lentiviruses encoding Cas9 were generated using the same technique. Culture supernatants were
770 harvested at 48 and 72 hours post transfection and used for infection (50% of Cas9-encoding virus +
771 50% of sgRNA-encoding virus) of MEFs, THP1 or Jurkat T cells together with polybrene (8 µg/ml)
772 using the spin-infection method. Cells were selected with puromycin (1 µg/ml) and blasticidin (5 µg/ml)
773 48 hours post infection. The sequences of the sgRNAs are described in Supplementary Table 1.

774 **Immunoprecipitation and immunoblotting.** For immunoprecipitation, cDNA encoding full-length or
775 fragments (a.a. 1-154 and 149-379) of FLAG-tagged STING and 6xHis-tagged STIM1 was transfected
776 into HEK293T cells. Transfected cells (2×10^7) were lysed in lysis buffer (20 mM Tris-Cl, 2 mM EDTA,
777 135 mM NaCl, 10% (vol/vol) glycerol, 0.5% Igepal CA-630, protease inhibitor mixture, pH 7.5) and
778 centrifuged at 100,000 x g for 1 hour before preclearing with protein G-Sepharose. Lysates were
779 immunoprecipitated with anti-FLAG antibody-conjugated resin for 6 hours. Immunoprecipitates were
780 washed five times in lysis buffer and analyzed by immunoblotting. For immunoblot analyses, cells
781 were lysed in RIPA buffer (10 mM Tris-Cl, 1% Triton X-100, 0.1% SDS, 140 mM NaCl, 1 mM EDTA,
782 0.1% sodium deoxycholate, and cOmplete Protease Inhibitor Cocktail [Sigma-Aldrich], pH 8.0) and
783 centrifuged to remove debris. Samples were separated on 8-10% SDS-PAGE. Proteins were
784 transferred to nitrocellulose membranes and subsequently analyzed by immunoblotting with relevant
785 antibodies. For dithiobis succinimidyl propionate (DSP) crosslinking, MEFs or HEK293T cells were left
786 untreated or treated with 0.125, 0.25, 0.5, or 1.0 mM of DSP for 1 hour on ice, followed by quenching
787 with 20 mM Tris-Cl, pH 7.5. Cells were lysed in SDS loading dye under non-reducing conditions
788 (without β-Mercaptoethanol) and separated on 10% SDS-PAGE and immunoblotted for detection of
789 indicated proteins. For endogenous immunoprecipitation, HEK293 cells were lysed in lysis buffer
790 (same as above) and centrifuged at 100,000 x g for 1 hour before preclearing with protein G-
791 Sepharose. Lysates were incubated with 2 µg of anti-STING antibody (Cell Signaling Technologies)

792 overnight and subsequently with protein G-Sepharose for 2 hours. For immunoprecipitation of STING
793 SAVI mutants with endogenous STIM1, HEK293T stably expressing FLAG-tagged human STING^{WT},
794 STING^{V147M}, STING^{N154S} or STING^{V155M} cDNAs were lysed in lysis buffer (same as above), centrifuged
795 at 100,000 x g for 1 hour, pre-cleared and incubated with anti-FLAG antibody-conjugated resin
796 overnight in lysis buffer containing 0.1% Igepal CA-630 and processed as described above. PBMCs
797 were lysed in NP40 Lysis Buffer (VWR Life Science) containing cOmplete Protease Inhibitor Cocktail
798 (Sigma-Aldrich) and centrifuged to remove debris. 20 µg of total protein from healthy control or patient
799 samples was separated on a 4-12% Bis-Tris Plus Gel (ThermoFisher), transferred to polyvinylidene
800 difluoride (PVDF) membrane and subsequently analyzed by immunoblotting with relevant antibodies.

801 **Purification of recombinant proteins from *E. coli*.** Full-length and fragments (a.a. 1-249, 250-400,
802 324-448, 400-600, and 600-685) of STIM1 were subcloned into pGEX4T-1 plasmid. GST fusion
803 protein expressing transformants were grown in liquid cultures and induced with isopropyl-1-thio-β-D-
804 galactopyranoside (IPTG, 0.2 mM) at 18°C overnight. Subsequently, cells were harvested and
805 resuspended in lysis buffer (50 mM NaH₂PO₄, 500 mM NaCl, 10% glycerol, pH 8.0) containing
806 protease inhibitors and 0.5% Triton X-100. Lysates were sonicated, centrifuged to remove debris and
807 incubated with glutathione sepharose 4B beads for 2 hrs. After washing 8 times with lysis buffer, the
808 beads were stored in lysis buffer without Triton X-100 at -20°C.

809 **GST pulldown analysis.** cDNA encoding full-length and fragments of STING-FLAG was transfected
810 into HEK293T cells. Transfected cells (2 x 10⁷) were lysed in lysis buffer (20 mM Tris-Cl, 2 mM EDTA,
811 135 mM NaCl, 10% (vol/vol) glycerol, 0.5% Igepal CA-630, protease inhibitor mixture, pH 7.5) and
812 centrifuged at 100,000 x g for 1 hour before preclearing with protein G-Sepharose. Lysates were
813 incubated with 20 µg of GST or GST-tagged fragments of STIM1 for 18 hours in binding buffer (0.5%
814 Igepal CA-630, 20 mM Tris-HCl, 100 mM NaCl, 2 mM EDTA, 10% glycerol, protease inhibitors, pH
815 7.5). Pulldown samples were washed five times with lysis buffer and analyzed by immunoblotting for
816 indicated proteins.

817 **HSV infection in mice.** Age and gender-matched control (*Stim1^{fl/fl}* or *Orai1^{fl/fl}*), *Stim1^{fl/fl}*Lyz2-cre or
818 *Orai1^{fl/fl}*Lyz2-cre mice were intravenously injected with 1×10^7 pfu of HSV-1 17+ strain. The viability of
819 the infected mice was monitored for 10 days. Mouse serum was collected at indicated times after
820 infection for measurement of serum cytokine by ELISA.

821 **Statistical analysis.** Statistical analysis was performed using the Origin2018b software (OriginLab,
822 Northampton, MA, USA). Data are presented as mean \pm s.e.m. For all dataset, normality and
823 homogeneity of variance were evaluated by Shapiro-Wilk test and Levene test respectively, to ensure
824 that the assumptions inherent to parametric significance testing were not violated. Statistical
825 significance to compare two quantitative groups was evaluated using two-tailed/unpaired t-test. When
826 multiple groups and/or multiple condition comparisons were necessary, one-way or two-way ANOVA
827 was performed followed by a Tukey HSD post-hoc test. Statistical comparison of multiple counts in
828 contingency tables was performed using Chi-square test followed by pairwise analysis of differences
829 as post-hoc test. A critical value for significance of $P < 0.05$ was used throughout the study, and
830 statistical thresholds of 0.05, 0.005 as well as 0.0005 are indicated in the figures by asterisks (see
831 legends for details).

832

833 **Data availability**

834 The data that support the findings of this study are available from the corresponding authors upon
835 request. The manuscript describing clinical phenotype of *STIM1* patient is available from OSR
836 Preprints (<https://doi.org/10.31219/osf.io/4duxt>).

837

838 **References**

- 839 37. Srikanth, S. *et al.* A novel EF-hand protein, CRACR2A, is a cytosolic Ca²⁺ sensor that
840 stabilizes CRAC channels in T cells. *Nat Cell Biol* **12**, 436-446 (2010).
- 841
- 842 38. Gwack, Y. *et al.* Hair loss and defective T- and B-cell function in mice lacking ORAI1. *Mol Cell*
843 *Biol* **28**, 5209-5222 (2008).

844

845 39. Stetson, D.B. & Medzhitov, R. Recognition of cytosolic DNA activates an IRF3-dependent
846 innate immune response. *Immunity* **24**, 93-103 (2006).

847

848 40. Srikanth, S., Jung, H.J., Ribalet, B. & Gwack, Y. The intracellular loop of Orai1 plays a central
849 role in fast inactivation of Ca²⁺ release-activated Ca²⁺ channels. *J Biol Chem* **285**, 5066-5075
850 (2010).

851

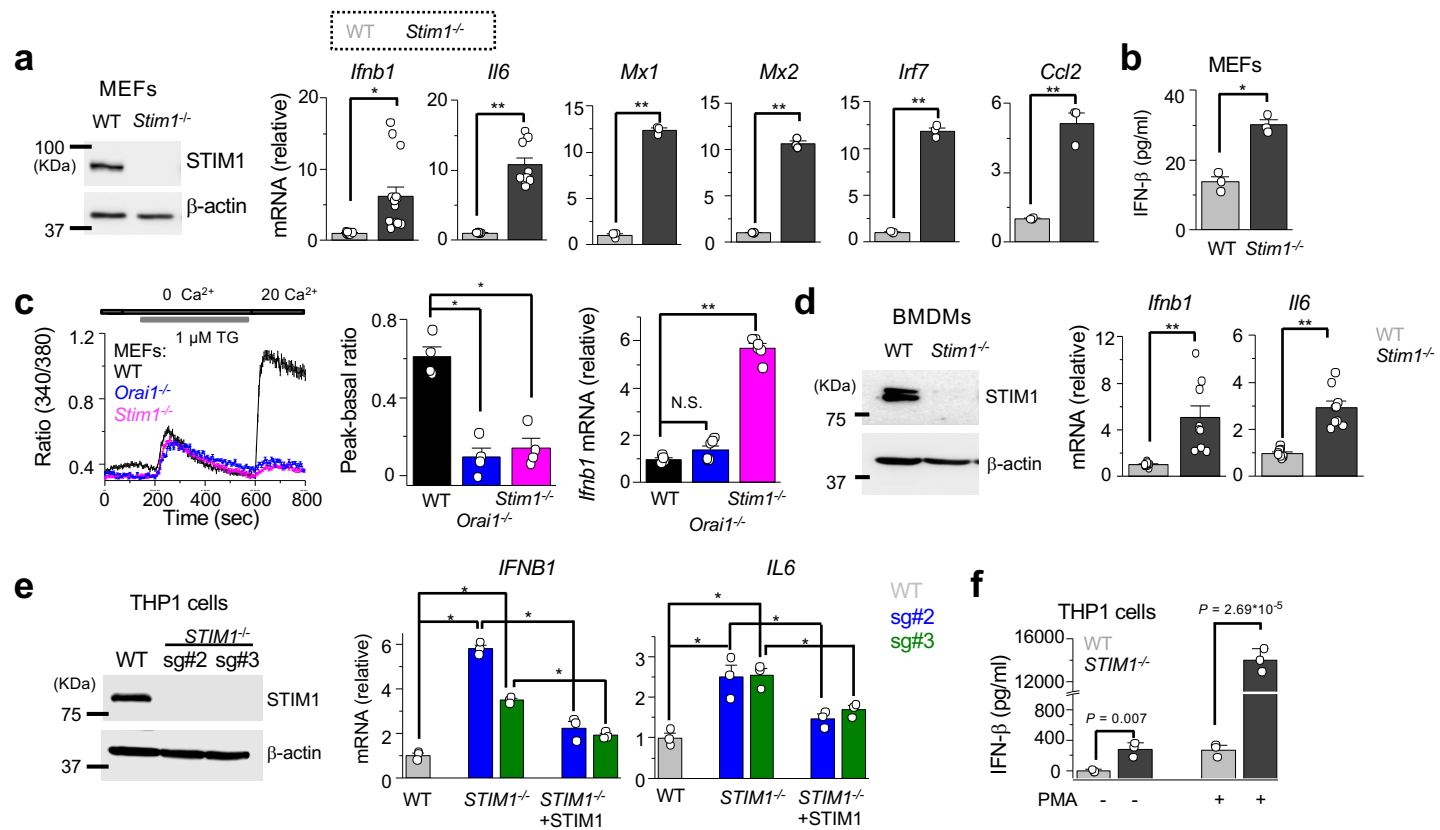


Figure 1

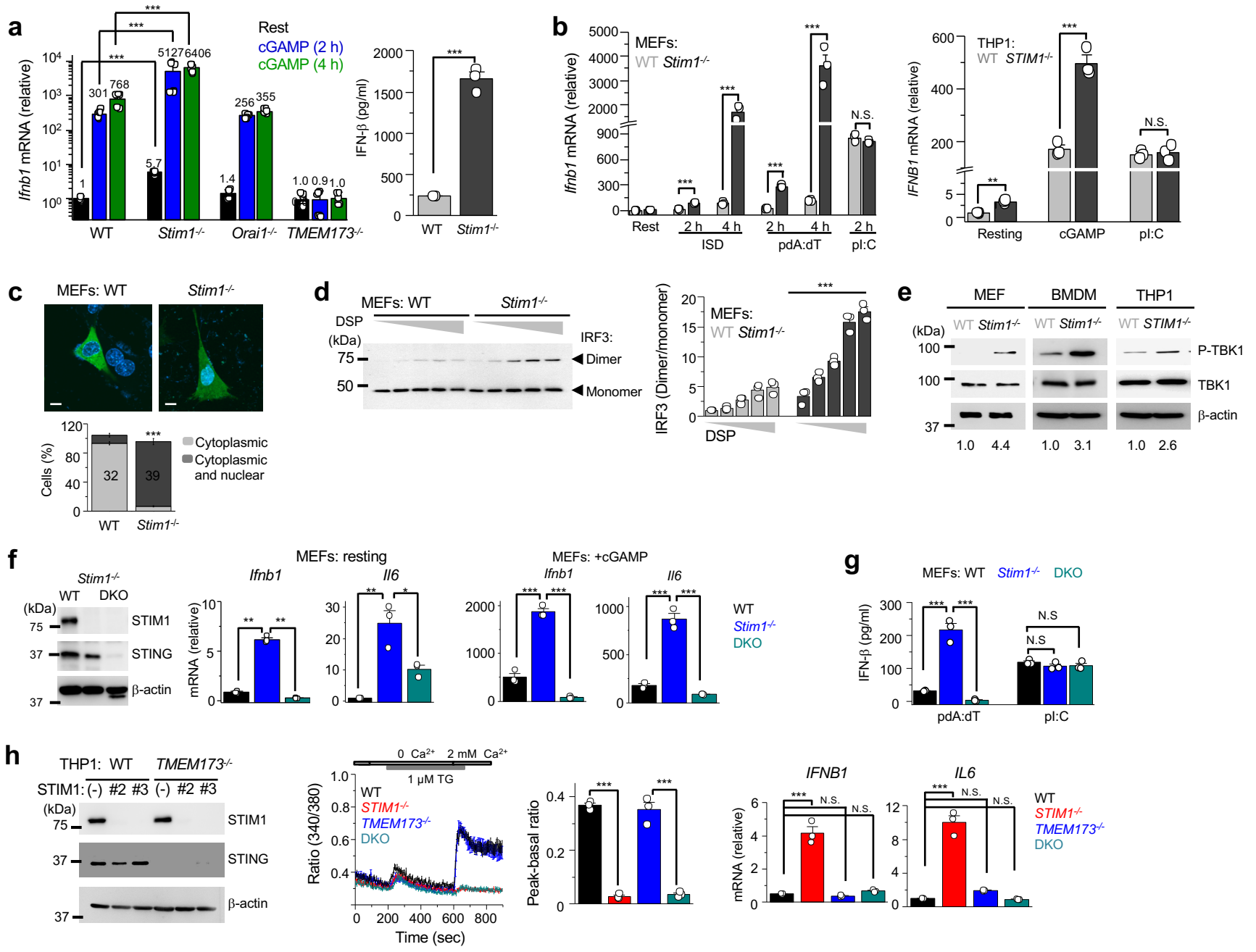


Figure 2

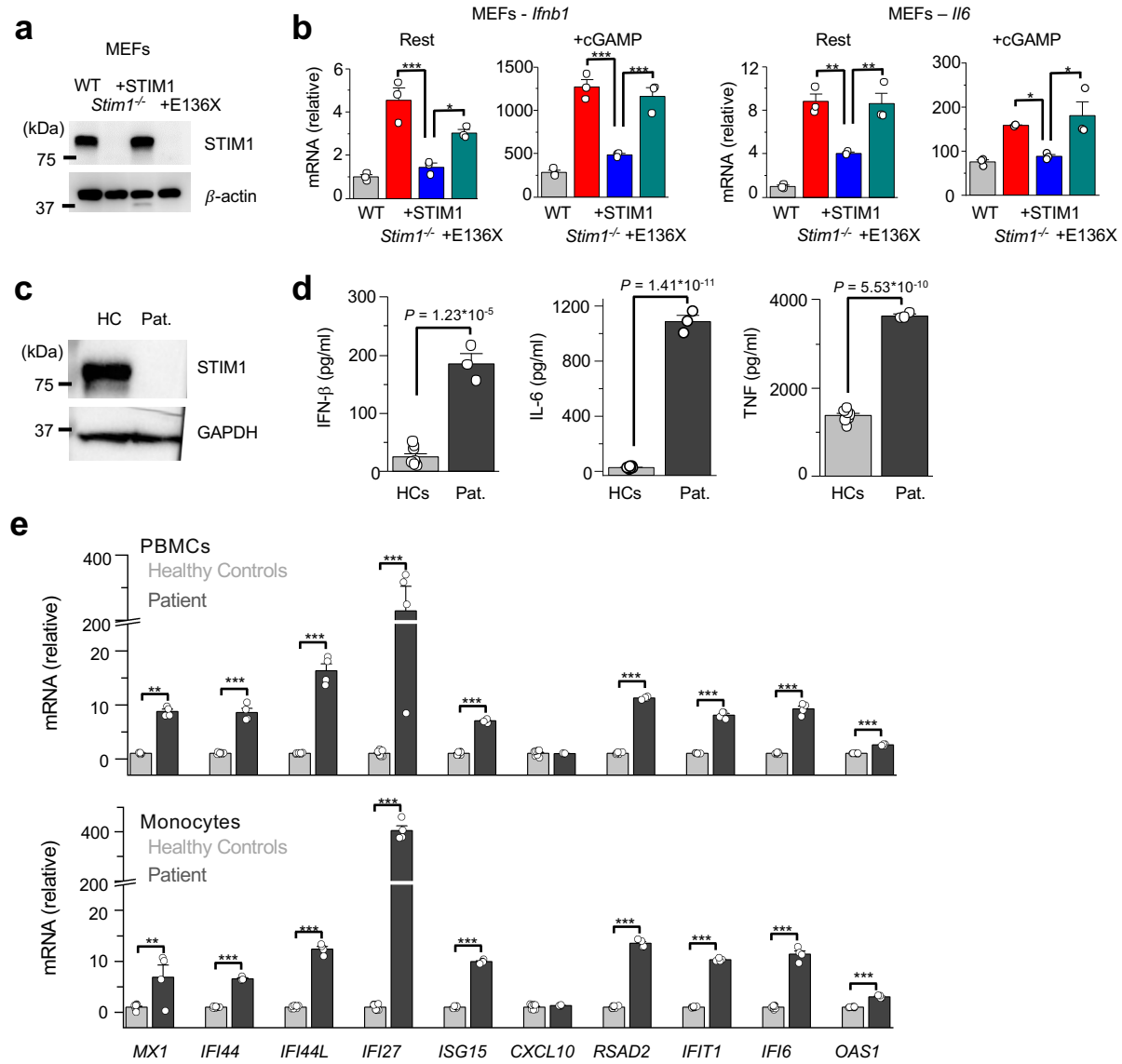


Figure 3

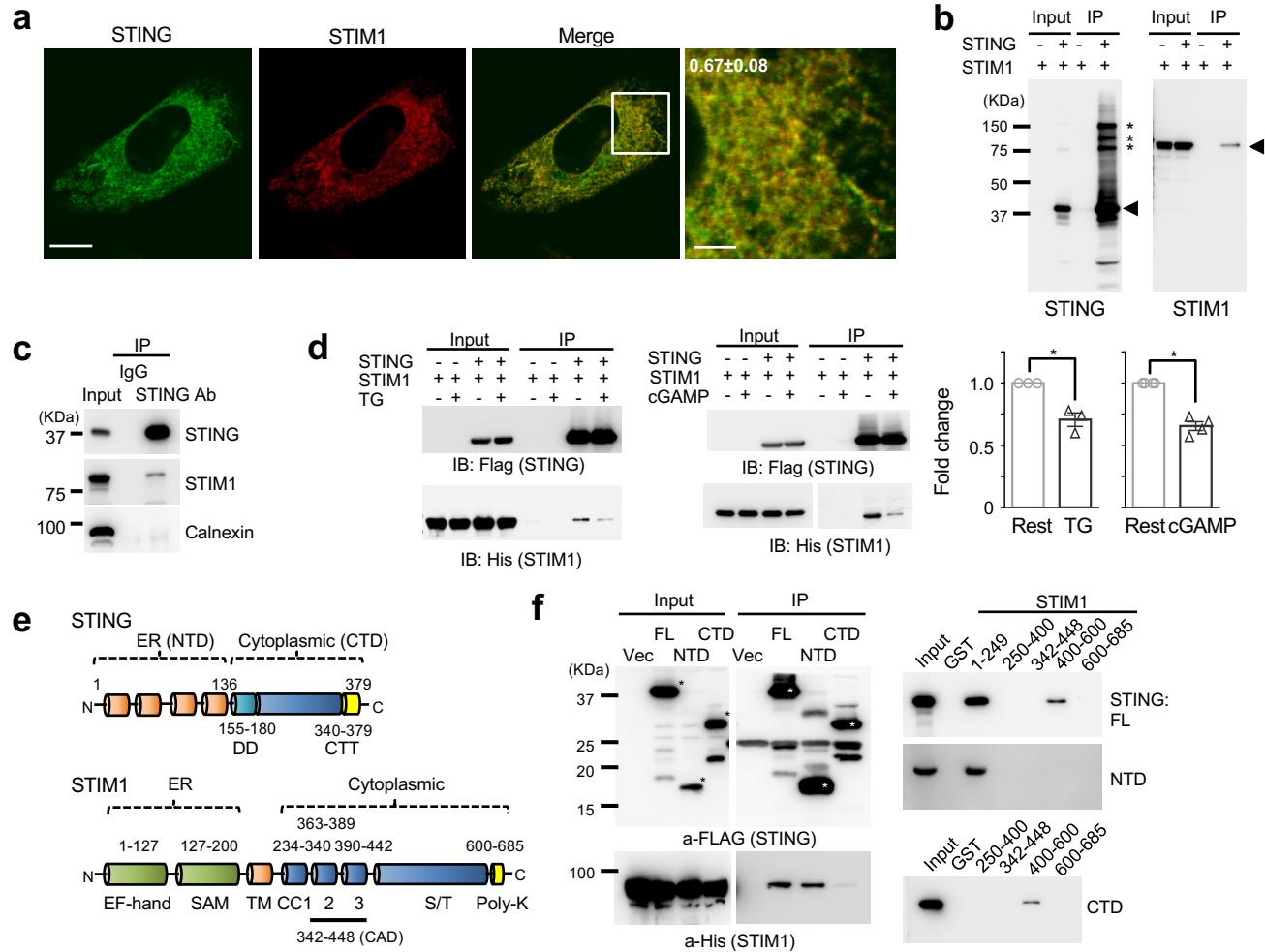


Figure 4

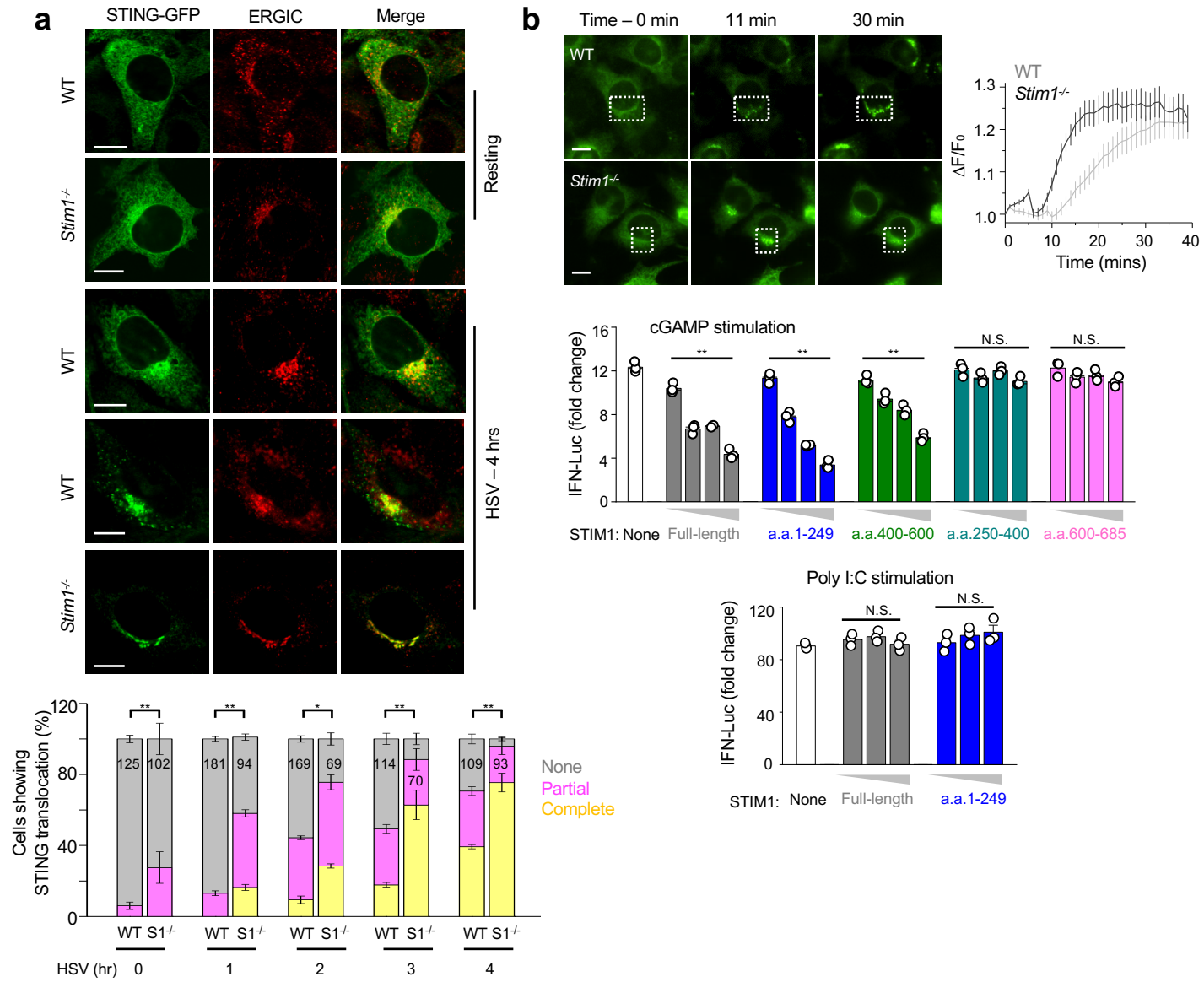


Figure 5

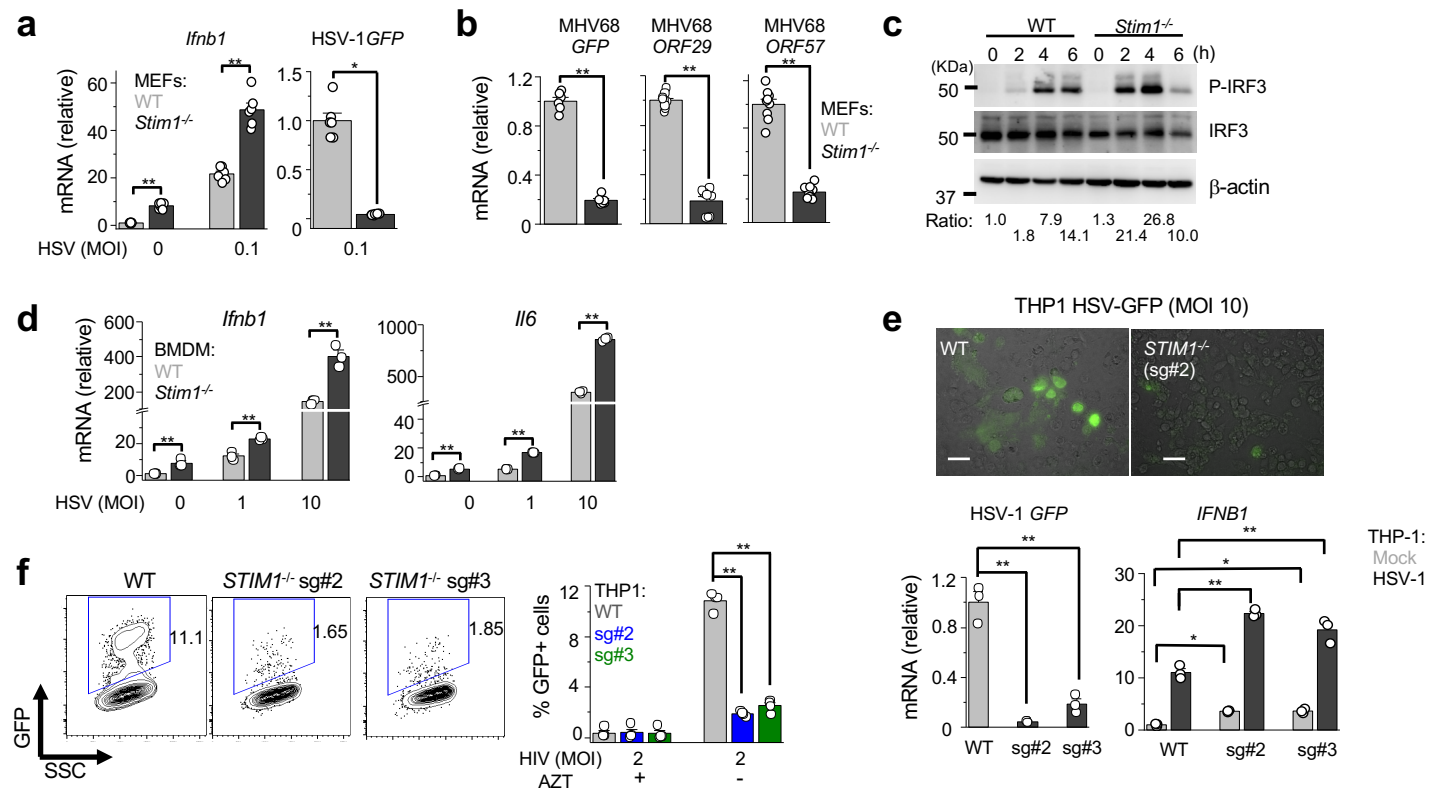


Figure 6

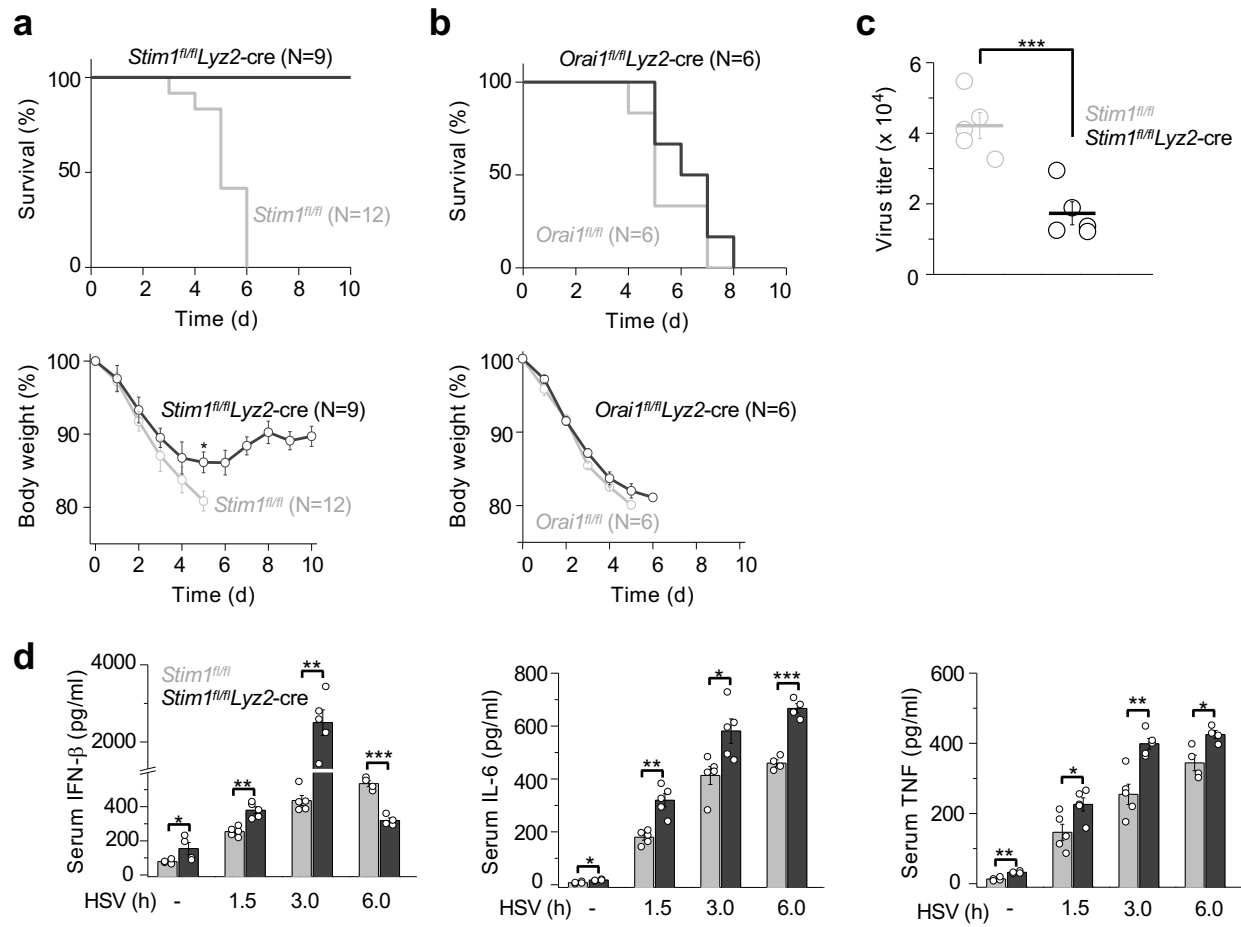


Figure 7